# **Deep-UV Conformable-Contact Photolithography for Bubble Circuits**

Abstract: The techniques of deep-ultraviolet(UV) conformable-contact photolithography are described and some preliminary work reported on their application to the fabrication of high-density bubble memory circuits by single-level masking. A quantitative analysis of tolerance requirements for linewidth, mask-to-wafer gap, and exposure is made for printing with conventional UV and deep-UV, for feature sizes in the range  $2.5~\mu m$  to  $0.1~\mu m$ . A new type of mask-to-wafer holder is described, utilizing a diaphragm to achieve contact. The holder can be used for either a conformable wafer or a conformable mask, or for both conformable wafer and mask, and for the liquid gap technique. Developmental bubble memory circuits on amorphous and garnet materials have been fabricated using deep-UV conformable-contact photolithography, electroplating, liftoff, and ion milling.

#### Introduction

Single-level masking, an inherently simple method of fabricating magnetic bubble memory circuits, requires a photolithographic technique capable of high resolution and high throughput. The experiments reported here show that conformable mask lithography at deep-ultraviolet (UV) wavelengths (2000 Å to 2600 Å) is a promising method for reproducing, from an electron-beam-fabricated mask, conductor lines and spacings less than one micrometer wide.

A printer operating at conventional UV wavelengths utilizes a light source, a condenser, and a mask-to-wafer holder. These basic components are retained in the deep-UV printer. However, because of the requirement to transmit in the deep-UV range, the glasses used for the condenser and mask substrate are replaced by quartz, sapphire, and fluoride optical materials. A new type of mask-to-wafer holder is also developed to ensure intimate contact.

High resolution, deep-UV conformable printing is a special case of diffraction printing [1], defined as a technique in which no focusing element exists between the mask and the wafer, and in which the dimension of the patterns on the mask is of the same order of magnitude as that of the printing wavelength. The resolution of diffraction printing is limited solely by diffraction, as the name implies. Therefore, when the minimum feature size (MFS) in a memory circuit is reduced in the submicrometer range, the allowable gap between the mask and the wafer decreases to a distance no larger than the thickness of the photoresist. This becomes an intimate-contact situation that can be achieved economically only by making one of the contacting elements conformable to the other, hence the name conformable-contact print-

ing. At wavelengths in the deep-UV range, the resolution and the gap tolerance of conformable-contact printing are further improved, e.g., 0.25- $\mu$ m lines can be obtained in the resist image having a height-to-width aspect ratio of seven, compared to an aspect ratio of 3.3 for printing at conventional UV wavelengths [2].

The conformable mask technique was first adopted by Smith [2-4]. Recently Hause and Sullivan [5] published their conformable-mask work in which a more sophisticated mask-to-wafer holder utilizes pressures larger than one atmosphere. In our work, conformable wafers with rigid masks as well as conformable masks with rigid wafers are used. The conformable wafer technique is more compatible for use with amorphous bubble materials and semiconductor device fabrication. Also, the use of the rigid mask lessens the risks of pattern dimensional change and accidental mask breakage. In addition, in previous work, conformable masks larger than the wafers were used to provide the pressure seal. We use masks and wafers of identical sizes instead, and a diaphragm for the pressure seal. The contact process is thus simplified. A conformable mask can be copied onto a rigid mask, or onto another conformable mask, and vice versa. The opaque and transparent parts on the mask can be interchanged or preserved, depending on whether liftoff or etching is used. These processes will be discussed in the next section.

Exploratory optical exposure of the well-known electron-beam resist [6] polymethyl methacrylate (PMMA) was reported by Moreau and Schmidt [7]. Bjorklund, Harris, and Young [8] used PMMA to record holograms at 1140 Å. We measured the deep-UV sensitivity and absorption coefficient of PMMA and found that a

213

Table 1 Simulation parameters of the PMMA and AZ photoresists. These data are used in the image evaluations in Figures 1 through 3.

	Deep UV, using photoresist PMMA 2041						Conventional UV, using photoresist AZ 1350J				
Wavelength (Å)	2050	2150	2250	2350	2450	2550	3130	3340	3660	4045	4358
Source intensity spectrum (relative)	2	8	13	22	30	29	84	60	192	136	169
Spectral photosensitivity (relative)	254.6	131.2	62.5	15.46	3.22	0.214	920	1680	1910	1820	1240
Refractive index	1.596	1.588	1.579	1.571	1.562	1.554	1.746	1.722	1.694	1.674	1.686

high-intensity illumination system can be built to reduce the exposure time to a practical interval. Hence, this photoresist material is mainly used in the present deep-UV fabrication studies. A detailed description of the characteristics of PMMA was published recently [9].

In the sections following, we discuss the resolution, gap, and intensity tolerances of diffraction printing, the deep-UV technique of conformable-contact printing, and the application of these techniques in the experimental fabrication of high-density bubble circuits.

## Theoretical prediction of performance of diffraction printing

As the minimum feature size in a circuit decreases, the special requirements of printing conditions, of course, become more stringent. These process parameters include wavelength, degree of perfection of contact, tolerance of illumination energy, and photoresist thickness. Because the limitations of MFS are so important, a theoretical analysis was made of image quality for various distances from mask to photoresist surface. Computations are made of diffraction patterns of circuit configurations, of constant-intensity profiles along the depth of the resist, and of the permissible gap tolerance between mask and wafer for various values of MFS. The analysis thus accounts for several printing conditions: conventional UV exposure, with a large mask-to-resist gap; deep-UV exposure; and intimate contact between mask and resist.

This analysis was done by simulation of diffraction printing images, which is complicated by several interacting parameters. As soon as the incident light reaches a pattern it produces a diffracted image everywhere, especially in the plane of the pattern [10]. It is absorbed in the photoresist and is multiply reflected at its surfaces. Moreover, as the photoresist is being exposed, the absorption coefficient decreases. We have succeeded in simulating diffraction images of one-dimensional line patterns from the plane of the mask to infinity, assuming perfectly conducting and infinitely thin opaque mater-

ial on the mask [10, 11]. Transverse electromagnetic waves, transverse magnetic waves, or unpolarized light can be used. Polychromatic radiation and an arbitrarily illuminating wavefront are treated as superposition of monochromatic plane waves. However, absorption, multiple reflection, and exposure saturation are neglected. Therefore, the simulation is more accurate for PMMA 2041 [12], which has an absorption coefficient [9] a factor of two smaller than that of AZ1350J [9, 13], for the transparent substrate, which has a refractive index matching that of the photoresist, and for low exposure levels.

The standard objects chosen for evaluation are:

- 1. A typical bar pattern consisting of three transparent bars of identical width and spaced by the same width.
- 2. A bar pattern in which the bars are separated by one-half of their width.

The former corresponds to chevron patterns and the latter to T-I bar patterns found in typical bubble memory circuits. The widths are 0.1, 0.25, 1.0, 2.0, and 2.5  $\mu$ m. An unpolarized plane wave is incident normal to the bar target. The intensity of the diffracted waves is computed at various distances from the plane of the mask. From these intensity distributions, the constant-intensity profile along the depth of the photoresist is plotted. Because the form of these profiles is related to the developed photoresist image, they are used for our theoretical performance evaluation.

The deep-UV spectrum from a Xe-Hg arc lamp, combined with the spectral photosensitivity of PMMA 2041 (corresponding to a solubility ratio of 100) given in Ref. [9], is taken to simulate the diffraction images. This continuous spectrum can satisfactorily be simulated by six discrete lines in the range 2050 Å to 2550 Å at 100-Å intervals. Decreasing the interval produces negligible changes. Similarly, conventional UV is simulated by the source spectrum of the Xe-Hg arc lamp combined with the spectral photosensitivity of AZ 1350J [14] at the five dominant Hg lines. The refractive indices of the

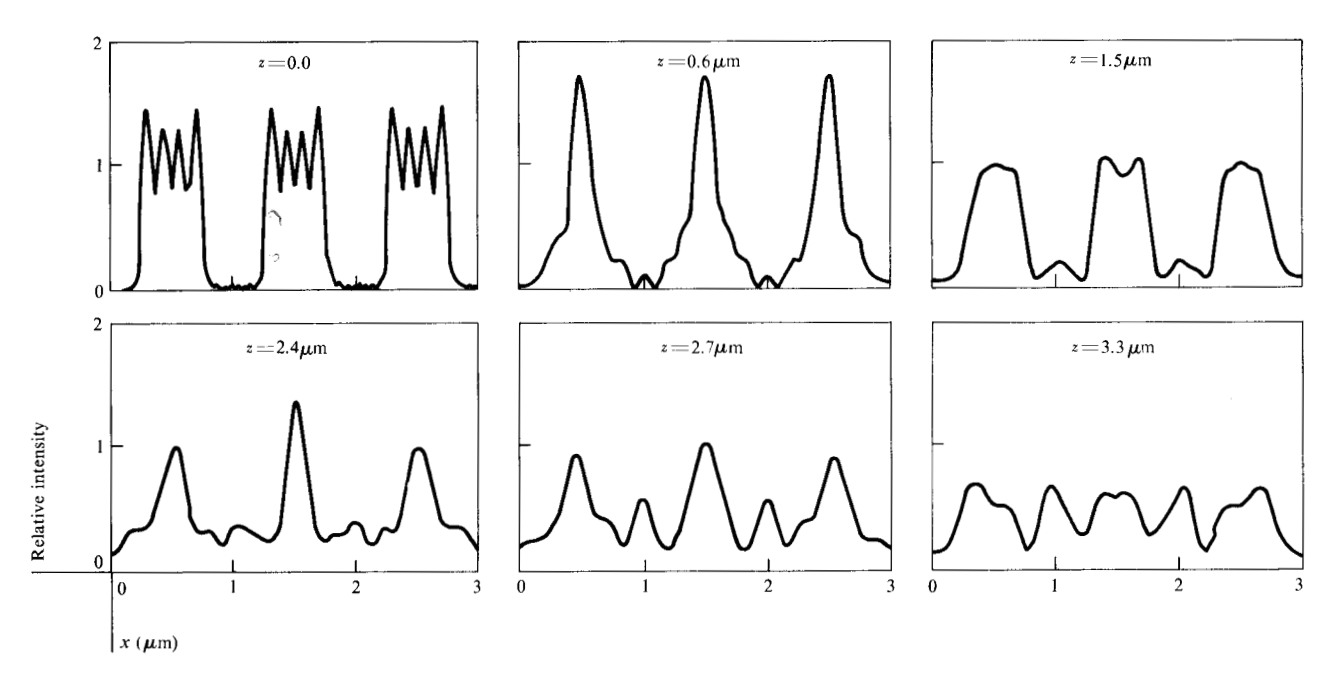


Figure 1 Computed diffraction patterns at various distances from a mask that contains 0.5-\mu m openings spaced 0.5 \mu m apart.

photoresists [15] were obtained from A. J. Warnecke with the apparatus described in Ref. [16]. These parameters are listed in Table 1.

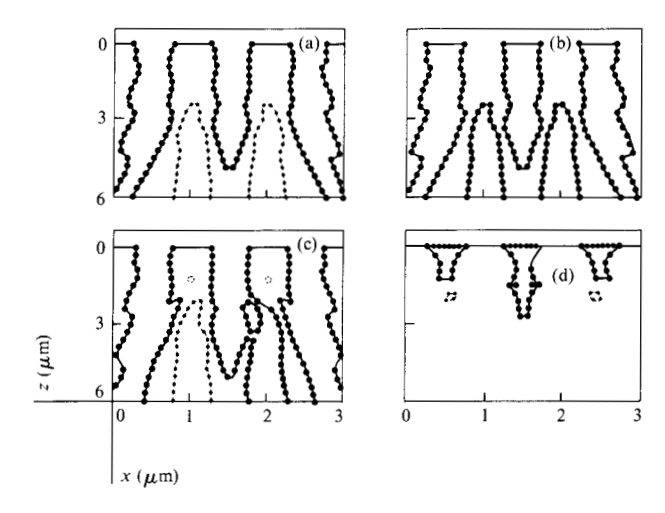
Sample diffraction curves of the 0.5- $\mu$ m bar target are shown in Fig. 1. At contact, the image is different from the intuitive geometric image. Because of the standing wave caused by the interference of the diffracted waves from the edges, the geometric image has many sharp peaks spaced a half-wavelength apart. Unpolarized illumination is used, and so the peaks are also found in the opaque regions of the mask. These peaks quickly disappear as the diffraction distance increases. At  $0.6~\mu$ m the image sharpens. It broadens at  $1.5~\mu$ m and then sharpens again at  $2.4~\mu$ m. At  $2.7~\mu$ m, the three main peaks become much lower while secondary peaks emerge. At  $3.3~\mu$ m, the secondary peaks dominate. A two-bar image results.

Sample constant-intensity profiles are shown in Fig. 2. They are represented by the cross section of a particular intensity level with the diffracted image at each of 20 distances from the mask. The reference intensity of one corresponds to the intensity of the normally incident plane wave. The profile in Fig. 2(d) shows the underexposed or undeveloped situation.

Increasing the exposure or the development time by a factor of 3.33 (assuming a reciprocal relationship between exposure and development) results in the situation shown in Fig. 2(c). The points at the left and the right side are purposefully joined asymmetrically, to demonstrate the two possible ways to interpret the cross sec-

tions. When the profile on the right-hand side results, the unsupported drop of unexposed photoresist is removed by the developer. Although overexposed or overdeveloped, the image shows a useful vertical profile for a photoresist thickness below two  $\mu$ m. In fact, from printing experience it is well known that the slant angle of an overcut profile [17] can be decreased by overexposure. However, because of the high absorption of the AZ photoresist, it is difficult to obtain vertical sidewalls simply by overexposing. A suitable profile for the liftoff process

**Figure 2** Computed constant-intensity profiles along the depth in photoresist. Relative intensities: (a) and (b), 2.86; (c), 3.33; (d), 1.00.



215

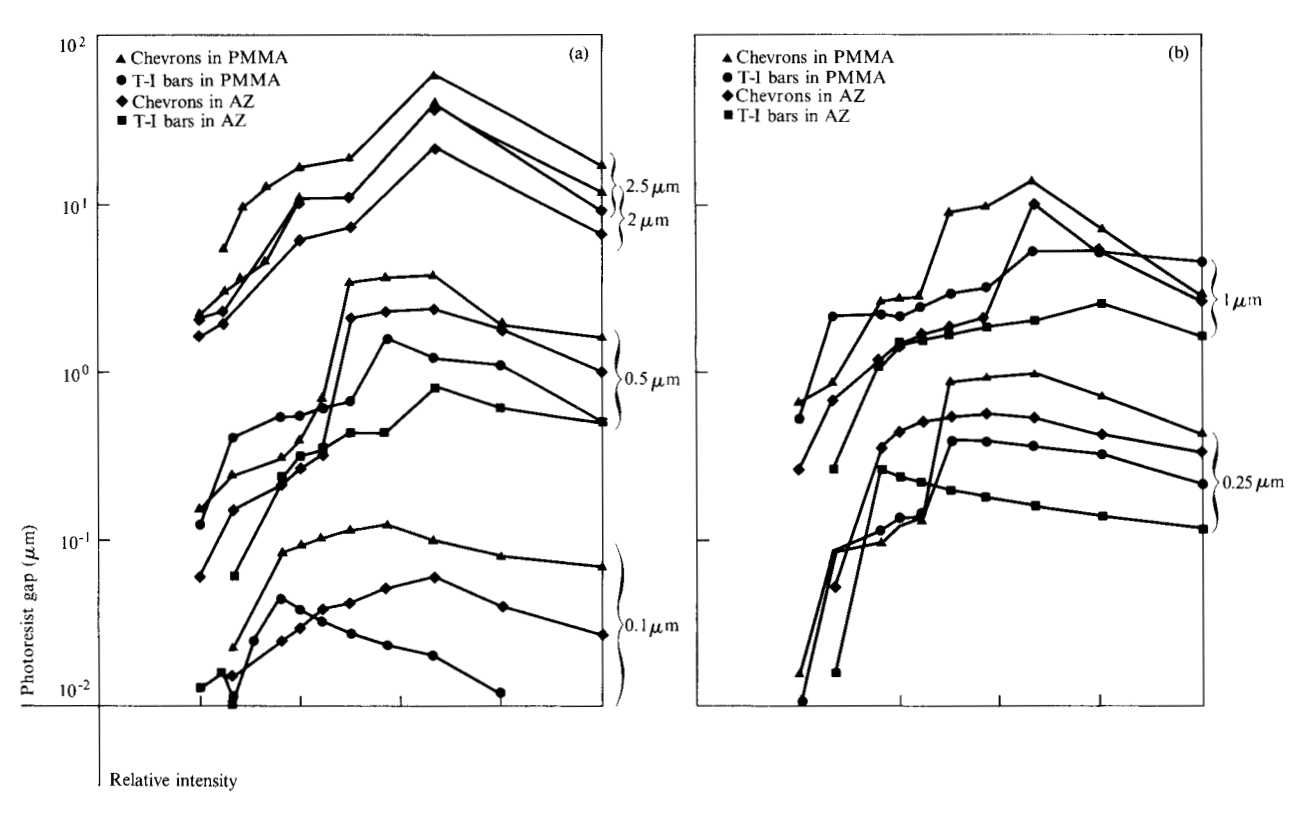


Figure 3 Computation of permissible photoresist gap vs intensity for various minimum feature sizes. The thickness of a combined air-and-photoresist gap can be evaluated by taking into account the respective refractive indexes.

can be obtained at intensity 2.86 shown in Fig. 2(a), where there is a bottleneck at 2.4  $\mu$ m. For PMMA, a proper combination of the ratio of width to absorption coefficient can result in vertical sidewalls or undercut profiles [17].

The regions enclosed by the dots shown in Fig. 2(a) are exposed and should be dissolved if they have not been protected by the unexposed photoresist. Therefore, at a depth of 4.8  $\mu$ m, the developed photoresist image still gives three bars, whereas the diffraction curves of Figs. 1 (e) and 1(f) indicate five bars. This demonstrates one of the reasons for the superiority of positive photoresists over negative photoresists. If a negative photoresist with similar optical parameters were used, the resultant developed image would resemble the constant-intensity profile shown in Fig. 2(b). The photoresist thickness here is limited to only 2.4  $\mu$ m.

The dependence of the maximum usable photoresist thickness on the fluctuation of the width of the image varies according to the metallization process adopted. For the liftoff process, the minimum width throughout the entire depth of the photoresist is crucial; for electroplating it is the width at the substrate, and for ion milling, the mean width. From the appearance of the typical

photoresist image shown in Fig. 2(a), it is obvious that smallest photoresist gap is allowed for the liftoff process, then ion milling, and finally electroplating. Here, we use the minimum-width criterion to determine the maximum usable photoresist thickness. A linewidth tolerance of  $\pm 30\%$  is used together with this minimum-width criterion to obtain the data in Fig. 3.

The gap tolerance of PMMA in Fig. 3 is larger than that of AZ for all feature sizes. The gap tolerance of chevrons is almost always better than that of T-I bars, except at low intensities. The smaller feature sizes require lower intensity. For a given mask with a variety of chevron and T-I patterns and feature sizes, this chart can be used to evaluate the optimum intensity to be used.

A typical photoresist image goes through several width fluctuations before it finally diminishes. When the  $\pm 30\%$  limit is shifted from one waist to another, an abrupt jump occurs in the curves of Fig. 3. The one- $\mu$ m AZ chevrons have an extraordinarily large gap tolerance because the jump at this particular pattern occurs at a shorter gap for PMMA.

The photoresist gap becomes as large as 60  $\mu$ m for 2.5- $\mu$ m PMMA chevrons. Because the optical absorp-

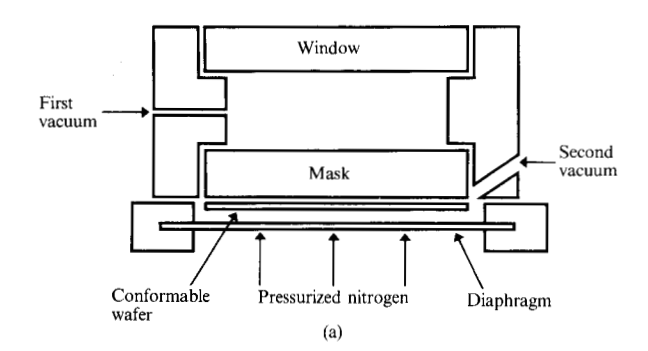
tion of PMMA makes high-resolution printing impractical beyond three  $\mu$ m, one has to convert the excess photoresist gap to an air gap that is smaller because of its lower refractive index.

#### Conformable-contact lithography

The classical way of achieving intimate contact, by pressing together two optically flat surfaces, is obviously not practical for contact printing. To achieve good contact, Smith [3] used a thin, flexible mask instead to conform to the wafer. The mask does not have to be optically flat but must be reasonably smooth. Dust particles and other imperfections outside the desired area do not deteriorate the diffraction image. Morever, since the contact pressure is evenly distributed, mask damage is greatly reduced. Using this conformable mask technique, Smith printed line patterns of 8000 Å periodicity through a 9800 Å layer of AZ 1350 photoresist.

To achieve adequate contact printing, we have developed a universal mask-to-wafer holder. It possesses the following capabilities:

- It takes either a conformable mask and a rigid wafer, or a rigid mask and a conformable wafer. Having one rigid element ensures easy separation after contact. If both elements are flexible, however, a strong seal is formed after intimate contact, which can be broken only by immersion in a liquid. In addition, being able to use conformable wafers makes the conformable printing technology compatible to amorphous bubble material and most semiconductor substrates. Lastly, a rigid mask is easier to handle, harder to break, and less susceptible to changes in dimension.
- 2. It does not use the conformable element to provide the vacuum seal, thus resulting in much less strain on the conformable element and permitting large thickness variation for the rigid element. In addition, a mask and wafer of the same size can be used. When 2) is combined with 1), rigid and flexible, positive and negative submaster masks can be fabricated from one single master mask of any type.
- 3. Besides the vacuum pressure, an independent positive pressure can be applied. The pressure can be used with the vacuum to promote contact. It is also necessary when a high-refractive-index fluid is used in the gap [18]. The vacuum used to hold the mask and the wafer evacuates the fluid too quickly. The fluid can be completely removed before the exposure is completed.
- 4. With these improvements, an interferometric study shows that typical silicon wafers 0.4 mm thick conform well, maintaining a gap less than one fringe wide across the entire 25-mm diameter field. Quartz plates as thick as 0.55 mm have also been successfully used.



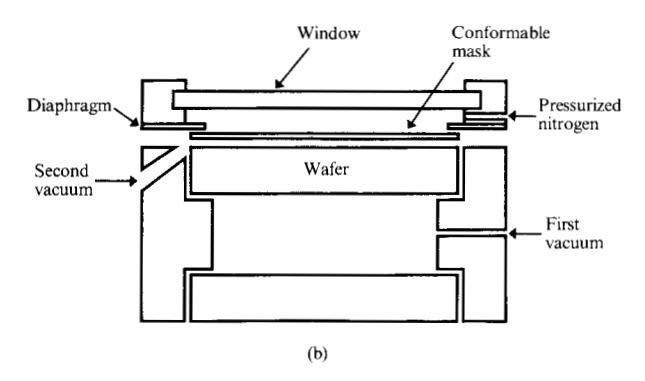


Figure 4 The mask-to-wafer holder. (a) Conformable wafer mode. (b) Conformable mask mode.

The holder is illustrated in Fig. 4 in the two modes of operation described, namely, the conformable mask and the conformable wafer modes.

Figure 4(a) shows the holder with rigid mask and a conformable wafer. The mask is held to the window assembly by the first vacuum, so that the mask can be handled easily. To achieve contact, the wafer is loaded on the diaphragm and then the mask assembly on the wafer. The second vacuum is then drawn, causing the diaphragm to move upwards to seal the opening and apply uniform pressure on the wafer. For tighter contact, positive pressure can be applied from below the diaphragm. When a high-refractive-index fluid is used, the second vacuum is not drawn, to avoid evacuating the fluid in the gap during exposure. Only the positive pressure is used to maintain intimate contact. After exposure, the second vacuum can be drawn to evaporate the fluid for easy separation of the mask and the wafer.

Figure 4(b) shows the holder with a conformable mask and a rigid wafer. It is the same holder as in Fig. 4(a) but turned upside down, with the wafer taking the position of the mask and vice versa. However, a full diaphragm would block the illumination. Therefore, a ring diaphragm with a pressurized chamber is added on top. The other operations are similar to those of the previous case.

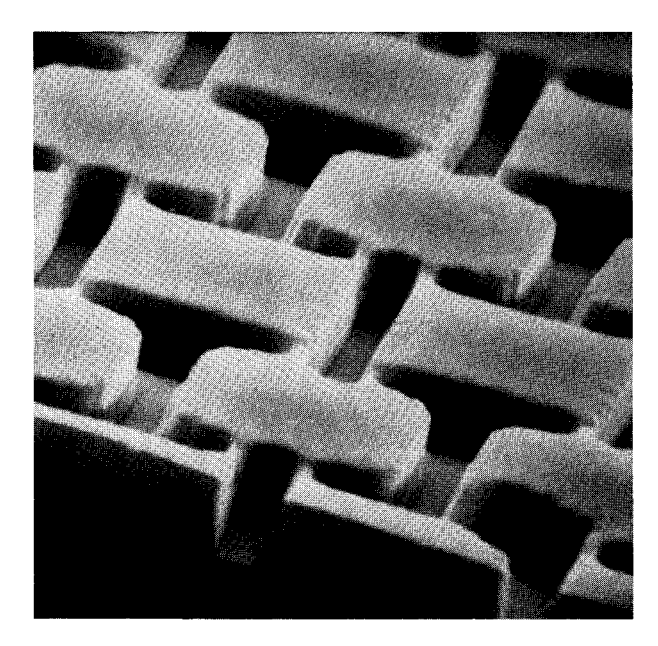


Figure 5 Scanning electron microscope picture of one-micrometer T-I bar openings in an AZ-1350 photoresist 3.6  $\mu$ m thick.

When unusual circumstances call for printing from conformable mask to conformable wafer, either mode of operation can be used with the addition of the thick supporting blank.

Figure 5 is a scanning electron microscope picture of one- $\mu$ m T-I bars in AZ 1350 photoresist 3.6  $\mu$ m thick. The intimate contact enables nine 2 mm  $\times$  2 mm chips, spaced 4 mm center-to-center, to be uniformly printed. The horizontal lines in the photoresist are due to standing waves caused by the interference of the image beam and the reflected beam from the wafer at the dominating 4050 Å Hg line.

#### Deep-UV lithography

As discussed in the first section, the wavelength of the printing light should be reduced, in order to increase the height-to-width aspect ratio in the developed photoresist and to allow imperfect contact. We have chosen the range 2000 Å to 2600 Å instead of the conventional range 3100 Å to 4500 Å, the new interval being the shortest possible without the complications of vacuum systems and unknown optical elements. Various aspects discussed here include the materials used, the choice of a light source with a suitable spectral characteristic, and the exposure time intervals.

#### • Photoresist

The key material for deep-UV lithography is a photoresist that is sensitive in this region. Few high-resolution photoresists respond below 3000 Å. Moreau and Schmidt [7] reported photoreaction in polymethyl meth-

acrylate (PMMA). Exposure of approximately an hour were required. However, PMMA is the most popular electron beam photoresist with well known coating, developing, and processing characteristics, and is therefore well worth serious consideration. Our sensitivity measurements indicated that a high-power illumination system can reduce the printing time to 4 to 10 minutes for a 38-mm diameter area through a typically one-μm thickness of PMMA 2041.

The spectral photosensitivity of PMMA 2041 [9] is of a reasonable order of magnitude. The long exposure, compared to that of AZ 1350J, is due to the low output from the mercury arc lamp in the region 2000 Å to 2600 Å. The sensitivity of PMMA 2041 becomes negligible at wavelengths above 2600 Å. Thus, the need for an expensive and lossy high-pass interference filter is eliminated.

#### • Source

A Hanovia 1-kW Xe-Hg arc lamp was chosen as the deep-UV source. Though its deep-UV output is only a small portion of its total radiation output, the absolute output in deep-UV is still the highest available, except, of course, for similar arc lamps with higher power ratings in the present experimental setup exposure times are between five and ten minutes for PMMA.

#### Mask

Fused quartz and sapphire are both transparent in deep UV. They are of considerable mechanical strength and are available in large diameters with a variety of thicknesses. We found them both suitable for the substrate of a deep-UV mask.

There are advantages and disadvantages for both chromium and aluminum. Chromium has good adhesion on quartz and is difficult to scratch. However, because of lower reflectivity and extinction coefficient, a larger thickness is required of chromium than of aluminum. The larger thickness presents mask fabrication problems when 0.125- $\mu$ m MFS is required by chemical etching. Aluminum has been found satisfactory for 0.25- $\mu$ m and 0.125- $\mu$ m masks.

Because aluminum is malleable it would appear to be susceptible to scratches. From our regular inspections, in which we do not seriously search for the increase of defects, a typical aluminum-on-quartz mask lasts approximately 50 prints in a standard laboratory atmosphere, without the setup of a clean room. Its durability is attributed mostly to the even distribution of stress in the intimate contact. Although too few samples have been run to date with chromium-on-quartz masks to provide any meaningful information, it is generally believed that they are more durable that the aluminum counterpart.

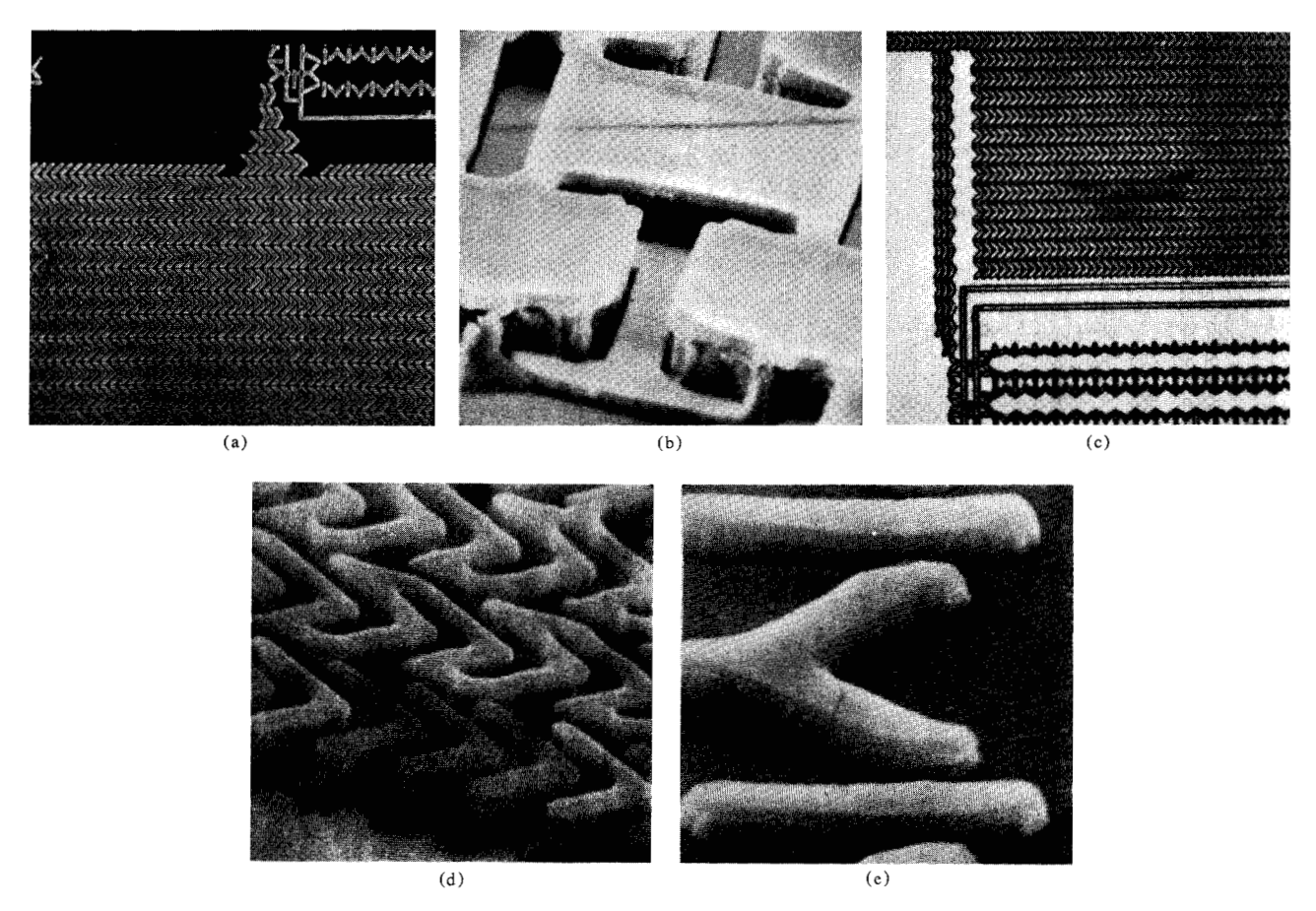


Figure 6 Bubble circuit patterns obtained by deep-UV conformable-contact lithography. Wafers in (a) to (d) are amorphous Gd-Co-Mo and in (e) are garnet. (a) Electroplated pattern of a magnetic bubble circuit. The Permalloy bars are 1.2  $\mu$ m wide and 3000 Å high. (b) Evaporated Permalloy layer on developed photoresist before liftoff. The bar width is 1  $\mu$ m. (c) Sputtered Permalloy and gold layers on bubble wafer. Unwanted metals and the photoresist have been lifted. The bar is 0.5  $\mu$ m wide and 6000 Å high. (d) Developed photoresist as an ion-milling mask. The bar is 0.5  $\mu$ m wide and 1.5  $\mu$ m high. (e) Permalloy bars on a bubble wafer after ion milling. The bar is 1  $\mu$ m wide and 3000 Å high.

### Fabrication of bubble circuits

Generally speaking, the single-level fabrication of masks requires a 3000-Å layer of Permalloy patterns and another 300 Å of similar conductor patterns on a film of magnetic bubble material.

The two metallic layers may be electroplated onto the bubble material. In this case, the thickness of the photoresist has to be only slightly more than that of the metals. For easy printing and good resolution, the photoresist thickness should be kept at a minimum. No photoresist residue should be left on the wafer.

The two metallic layers can also be fabricated by the liftoff process. In this case, the thickness of the photoresist has to be considerably larger than 6000 Å. In practice, more than 8000 Å is required. The profile of the developed photoresist has to be either vertical or undercut. Otherwise, the desired part of the metals cannot be separated from the rest. We have been able to

obtain vertical side walls in a single layer of PMMA 2041. Therefore there is no loss in resolution in our lift-off process. As in the previous case, no photoresist residue is allowed.

The two metallic layers can be predeposited and the unwanted portions can then be ion-milled, using the photoresist as a mask to protect the wanted part. In this case, the ion-milling parameters and the photoresist thickness are closely related. Therefore, the thickness should be carefully controlled. In order to obtain vertical sidewalls on the metallic layer, the sidewalls of the photoresist should be kept vertical. In this case, however, some slight residue of photoresist is permitted.

The magnetic bubble materials used here are usually either Gd-Co-Mo or garnet. The amorphous Gd-Co-Mo is evaporated onto glass substrates, 0.25 mm thick, which are conformable and are printed in the conformable wafer mode. The garnets are usually grown on 0.75-

mm-thick substrates and therefore are usually printed in the conformable mask mode. Although either deep-UV lithography or conformable printing is adequate for printing the one- $\mu$ m lines and 0.5- $\mu$ m spacings, the process of the combined technique has been used to permit relaxed tolerances.

#### **Experimental results**

Figure 6 illustrates patterns photographed with scanning electron microscopy. Figure 6(a) shows a part of magnetic bubble memory circuit consisting of 1.2- $\mu$ m Permalloy bars spaced less than  $0.3~\mu$ m apart on amorphous material. A rigid 3.2-mm-thick aluminum-on-quartz opaque background mask and 4000~Å of PMMA 2041~was used. The nickel-iron Permalloy bars were deposited by electroplating.

Figure 6(b) shows the preparation for the liftoff process. The Permalloy was evaporated on the photoresist and the bubble material, resulting in the configuration shown. The profile of the photoresist openings should be vertical or slanted so that the Permalloy on the photoresist and the Permalloy on the bubble material are discontinuous, enabling the unwanted permalloy to be washed off with the photoresist later.

Figure 6(c) shows part of a bubble memory circuit in which the metals have already been lifted off. The width of the bars and the gaps between them are intended to be 0.05  $\mu$ m and 0.25  $\mu$ m, respectively. Permalloy and gold, each layer of 3000 Å thickness, were deposited by sputter gun [19]. A rigid aluminum-on-quartz, opaquebackground mask 3.2  $\mu$ m thick and a 1.2  $\mu$ m layer of PMMA 2041 were used.

Figure 6(d) shows developed 0.5- $\mu$ m chevron patterns spaced 0.25  $\mu$ m apart in a 1.2- $\mu$ m layer of photoresist, intended to be an ion-milling mask to protect the wanted areas in the uniform Permalloy layer underneath. A conformable aluminum-on-quartz, transparent-background mask 0.25 mm thick was used. In this case, both the mask and the wafer are conformable. The mask-wafer holder was used in the conformable wafer mode with a rigid quartz blank above the conformable mask. Figure 6(e) shows 1- $\mu$ m Permalloy bars after ion milling.

#### Concluding remarks

An experimental deep-UV conformable printing technique is described. Its ultimate limitations are predicted theoretically and some preliminary fabrication results on single-level bubble circuits are reported.

The work described here does not include an alignment setup, which would be required for multilevel bubble circuits or semiconductor circuits. Because of the similarity to conventional contact printers, a comparable alignment accuracy for those applications can be

reasonably anticipated. However, to utilize the ultimate resolution capability, which requires alignment accuracy of  $0.03~\mu m$  ( $\frac{1}{4}$  of the resolution), new methods will have to be found. An electron microscope is needed for viewing but this would drastically increase the installation cost. It could be justified only by the high throughput and the large aspect ratio of height to width. Of course, for all high-resolution uses the original mask has to be made by electron-beam fabrication. The aspect ratio can then be amplified with deep-UV conformable printing. The full-wafer processing advantage of deep-UV conformable printing is not possible if a significant dimensional change in the wafers occurs after heat processing. These various handicaps, however, are of no concern for single-level bubble circuits.

Because of the intimate contact, the probability of mask damage is inherently higher than for other, non-contact printing technologies. This could be minimized to a practical level by carefully controlling the cleanliness of the printing environment, and by using wave-guiding mask protective layers [20].

#### Acknowledgments

The author is indebted to the support given by J. S. Wilczynski on optical projection systems, W. G. Santy on the mask-wafer holder, W. M. Moreau and M. Hatzakis on photoresist, and L. J. Tao, K. Y. Ahn, J. V. Powers, and M. S. Cohen on bubble circuit fabrication. He appreciates having the very high quality electron-beam mask made by T. P. Chang, H. E. Luhn, and M. Hatzakis. Consistent encouragement and consultation by A. N. Broers and J. S. Wilczynski are gratefully received.

#### References and notes

- The term "diffraction printing" is defined to include the diffraction-limited part of contact and proximity printing and to exclude x-ray lithography. Diffraction printing covers the case in which the image to printed is exactly on the mask, because this image is already a diffracted image and is quite different from the image formed by geometrical optics. When the dimension of the feature becomes large compared with wavelength, shadow printing takes place.
- H. L. Smith, N. Efremow, and P. L. Kelly, "Photolithographic Contact Printing of 4000 Å Linewidth Patterns," J. Electrochem. Soc. 121, 1503 (1974).
- H. L. Smith, "Method for Fabricating High Frequency Surface Wave Transducers," Rev. Sci. Instr. 40, 729 (1969).
- J. Melngallis, H. L. Smith, and N. Efremow, "Instrumentation for Conformable Photomask Lithography," *IEEE Trans. Electron Devices* ED-22, 496 (1975).
- F. L. Hause and P. A. Sullivan, "Conformable Mask Photolithography," SPSE Symposium on Micro-Photofabrication, Palo Alto, California, February, 1975.
- M. Hatzakis, "Electron Resists for Microcircuit and Mask Production," J. Electrochem. Soc. 116, 1033 (1969).
- W. M. Moreau and P. R. Schmidt, "High Resolution Proximity Printing," 1038th Electrochemical Society Meeting, extended abstract no. 187, 1970.
- G. C. Bjorklund, S. E. Harris, and J. F. Young, "Vacuum Ultraviolet Holography," Appl. Phys. Lett. 25, 451 (1974).

- 9. B. J. Lin, "Deep-UV Lithography," J. Vac. Sci. & Technol. 12, 1317 (1975).
- B. J. Lin, "Near-Field Diffraction of a Medium Slit," J. Opt. Soc. Am. 62, 977 (1972).
- B. J. Lin, "Near-Field Diffraction of Bar Targets, Gratings, and Fresnel Zone Plates," J. Opt. Soc. Am. 64, 528A (1974).
- 12. 2041 is the grade number given to the Dupont product Elvacite®. The other popular PMMA resist, Elvacite 2010, is of lower molecular weight and has a higher unexposed dissolution rate and thus a smaller exposure latitude.
- 13. F. H. Dill, W. P. Hornberger, P. S. Hauge, and J. M. Shaw, "Characterization of Positive Photoresist," *IEEE Trans. Electron Devices* ED-22, 445 (1975).
- 14. The spectral photosensitivity of AZ 1350J was evaluated by the method described in Ref. 9.
- The refractive indexes of PMMA 2010 and AZ 1350H were used because of the unavailability of data for PMMA 2041 and AZ 1350J.
- A. J. Warnecke and P. J. LoPresti, "Refractive Index Dispersion in Semiconductor-related Thin Films," *IBM J. Res. Develop.* 17, 256 (1973).

- 17. An overcut profile is that which has a large linewidth at the surface and a narrow linewidth at the bottom. An undercut profile is the opposite.
- 18. When there are raised features on the wafer, as in multiple-level devices, the effective optical distance between mask and photoresist can be reduced by inserting a fluid of high refractive index. This technique is also desirable when air bubbles become a limitation for masks with a low-MFS requirement.
- 19. P. Clark, U.S. Patent Nos. 3,616,450 (1971) and 3,711,398 (1973).
- W. M. Moreau and H. R. Rottmann, "Optical Mask with Integral Spacers and Method of Making," U.S. Patent No. 3,676,002 (1972).

Received April 30, 1975

The author is located at the IBM Thomas J. Watson Research Center, Yorktown Heights, New York 10598.